ACS APPLIED MATERIALS & INTERFACES

Research Article

www.acsami.org

Conformal and Highly Luminescent Monolayers of Alq_3 Prepared by Gas-Phase Molecular Layer Deposition

André Räupke,[†] Fabian Albrecht,[‡] Julia Maibach,[§,∥] Andreas Behrendt,[†] Andreas Polywka,[†] Ralf Heiderhoff,[†] Jonatan Helzel,[‡] Torsten Rabe,[‡] Hans-Hermann Johannes,[‡] Wolfgang Kowalsky,[‡,§] Eric Mankel,[§,∥] Thomas Mayer,[§,∥] Patrick Görrn,[†] and Thomas Riedl*[,†]

[†]Institute of Electronic Devices, University of Wuppertal, 42119 Wuppertal, Germany

[‡]Institute of High-Frequency Technology, Technical University of Braunschweig, 38106 Braunschweig, Germany

[§]InnovationLab GmbH, Speyerer Straße 4, 69115 Heidelberg, Germany

[∥]Institute of Materials Science, Surface Science Division, Technische Universität Darmstadt, Petersenstraße 32, 64287 Darmstadt, Germany

Supporting Information

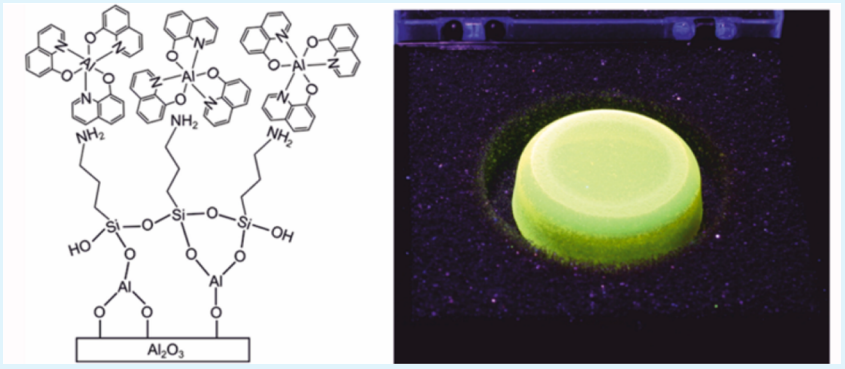

ABSTRACT: The gas-phase molecular layer deposition (MLD) of conformal and highly luminescent monolayers of tris(8-hydroxyquinolinato)aluminum (Alq_3) is reported. The controlled formation of Alq_3 monolayers is achieved for the first time by functionalization of the substrate with amino groups, which serve as initial docking sites for trimethyl aluminum (TMA) molecules binding datively to the amine. Thereby, upon exposure to 8-hydroxyquinoline (8-HQ), the self-limiting formation of highly luminescent Alq_3 monolayers is afforded. The growth process and monolayer formation were studied and verified by in situ quartz crystal monitoring, optical emission and absorption spectroscopy, and X-ray photoelectron spectroscopy. The nature of the MLD process provides an avenue to coat arbitrarily shaped 3D surfaces and porous structures with high surface areas, as demonstrated in this work for silica aerogels. The concept presented here paves the way to highly sensitive luminescent sensors and dye-sensitized metal oxides for future applications (e.g., in photocatalysis and solar cells).

KEYWORDS: *molecular layer deposition, Alq_3, surface functionalization, sensitized surfaces, gas-phase deposition*

INTRODUCTION

Monolayers of organic molecules with electro-optical functionality play an important role in a number of applications, for example, dye-sensitized solar cells (DSSC),[1] sensitizing metal oxides for catalysis,[2] and highly sensitive luminescent sensors[3] for explosives, drugs, or bioanalytes. Typically, these electro-optically active molecular monolayers are prepared from solution. This approach faces severe limitations in cases where the substrate to be coated does not tolerate the use of a solvent or if the dye molecule itself is not sufficiently soluble. If highly porous samples are to be coated in a solution process, the subsequent removal of the solvent may become an additional issue. Thus, it is desirable to prepare monolayers of functional molecules from the gas phase. Following this line of thought, molecular layer deposition (MLD) has recently been envisaged as a solvent-free approach to create organic molecular layers with a similar level of control and perfection as that of inorganic films prepared by atomic layer deposition (ALD).[4] In both MLD and ALD, the deposition process relies on the sequential (either temporal or spatial) exposure to two reactants (precursors), which undergo self-limiting chemical reactions at the surface to be coated. Thereby, they form the desired material in a layer-by-layer fashion even on very complex high-aspect-ratio surfaces.[5,6] Although ALD is a low-pressure (1 mbar) coating technique, atmospheric pressure processes have been reported very recently, rendering the

Received: November 4, 2013
Accepted: December 19, 2013
Published: December 19, 2013

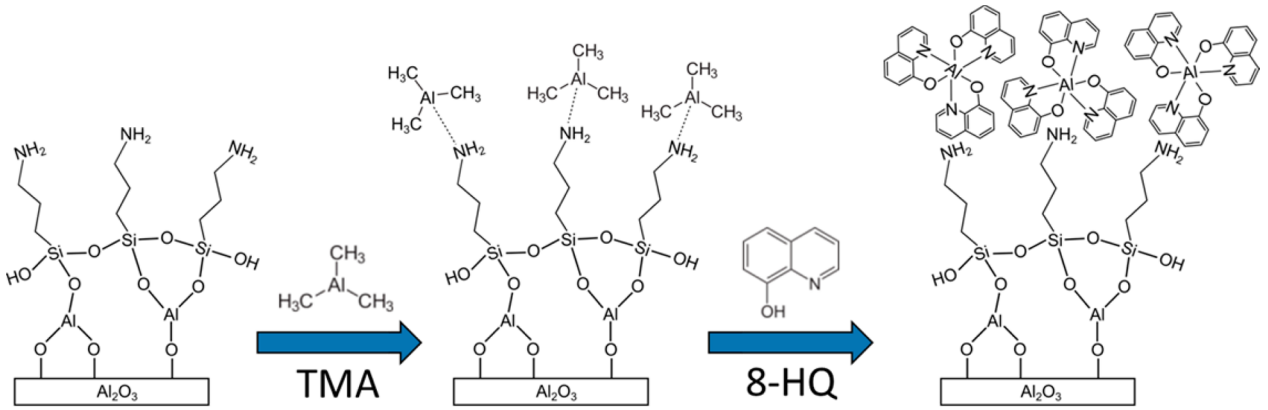

Figure 1. Schematic for the preparation of Alq_3 monolayers in an MLD process.

ALD/MLD technique attractive for cost-effective production and even for roll-to-roll manufacturing.[7,8] A plethora of MLD processes for passive organic molecules without particular active electro-optical functionality have been demonstrated.[9−11] In particular, hybrid materials made from typical ALD precursors and alcohols, so-called metalcones, have received considerable attention because of their tunable electrical, optical, and mechanical properties.[12] As of yet, there is only very limited work on the MLD of molecular systems that allow for functionalities like charge transport or luminescence. Yoshimura et al. reported quantum size effects in the optical absorption spectra of molecular azomethine wires with controlled variation of the wire length.[13] Burtmann et al. studied quantization effects in the electro-optic properties in few layers of 1,8:4,5-naphthalenetetracarbodiimide (NTCDA) grown by MLD.[14] The MLD growth of thick layers (few 100 nm) of luminescent metal quinolinates (Mq_x) has been investigated by the group of Nilsen.[15,16]

In this work, we present an avenue for the controlled preparation of conformal and highly luminescent monolayers of tris(8-hydroxyquinolinato)aluminum (Alq_3). Alq_3 can be considered the fruit fly of organic optoelectronics: it was the electron transporter and luminescent material in the first efficient heterostructure organic light-emitting diode (OLED) demonstrated by Tang et al.[17] In our work, the controlled formation of Alq_3 monolayers is achieved by functionalization of the substrate with amino groups, which serve as initial docking sites for trimethyl aluminum (TMA) molecules that datively bind to the amine. Subsequent exposure to 8-hydroxyquinoline (8-HQ) affords the self-limiting formation of highly luminescent Alq_3 monolayers on arbitrary surfaces (e.g., curved 3D objects or highly porous silica aerogels). This concept will be generally applicable for the preparation of other monolayers of luminescent metal quinolinates. As a case study, the Alq_3 monolayers prepared in this work were used to sensitize TiO_2 surfaces with a high surface area.

EXPERIMENTAL SECTION

As substrates, we used silicon wafers with native oxide or Borofloat glass. All substrates were cleaned before deposition in a solution of deionized water (96% v/v), pure citric acid (2% v/v), and EXTRAN neutral from Merck (2% v/v). Subsequently, the substrates were rinsed with deionized water. Finally, the substrates were rinsed with isopropyl alcohol and blown dry with nitrogen. Silica aerogel was obtained from Aerogel Technologies LLC and used as received.

For the ALD/MLD deposition, we used a home-built reactor using nitrogen as carrier gas (background pressure 0.4−1 mbar). For in situ quartz crystal microbalance (QCM) measurements, high-temperature $GaPO_4$-based quartzes (R-20 SuperQuartz, Piezocryst) were used. As precursors for ALD/MLD deposition, we used trimethylaluminum (TMA) (98%+, from ABCR), titanium chloride (99.9%, Sigma-Aldrich), tetrakis (dimethylamido)zirconium (TDMAZ) (95%+, Fisher Scientific), (3-aminopropyl)triethoxysilane (APTES) (99%, Sigma-Aldrich), and 8-hydroxyquinioline (8-HQ) (99%, Sigma-Aldrich). For the deposition of Al_2O_3, we used a N_2 carrier gas flow of 145 sccm, resulting in a reactor pressure of 0.9 mbar. Both H_2O and TMA precursors were kept at room temperature, and the dosing time was 50 ms for both followed by a 30 s purge. For the organic deposition, the reactor pressure was 0.4 mbar. The APTES and 8-HQ precursors were kept at 75 and 100 °C, respectively. APTES and 8-HQ were dosed for 2.5 s followed by 120 and 240 s purge, respectively.

For the thermal evaporation of reference Alq_3 layers, we used a commercial vacuum-coating system (Edwards AUTO 306 Vacuum Coater) at a base pressure of about 5×10^{-7} mbar. As a source material, sublimed-grade Alq_3 (99.995%) from Sigma-Aldrich was used.

As the excitation source for the photoluminescence measurements, we used a frequency tripled, cw DPSS laser (λ = 355 nm, optical output power = 10 mW). PL spectra were acquired using a grating monochromator (Princeton Instruments Acton SP2500) and a thermo-electrically cooled CCD camera (Princeton Instruments Pixis 100) as detector.

Time-resolved PL data has been acquired by a streak camera system (Hamamatsu 4334 with Chromex spectrometer, time resolution ∼2 ps). As the excitation source, a subnanosecond, frequency tripled DPSS laser was used (AOT, λ = 355 nm).

The spectral absorption/transmission measurements were carried out using a white deuterium Halogen lamp (DH-2000-BAL, Ocean Optics, 1 mW cm^{-2}) as a source and a fiber spectrometer (USB 2000+XR1-ES, from 186 to 1041 nm) as detector. Each spectrum is an average of about 200 measurements on 10−20 different sample positions.

The scanning electron microscopy study was done using a Philips XL30S FEG microscope with a field-emission cathode.

The photoelectron spectroscopy characterization was performed using a PHI VersaProbe II scanning XPS microprobe located at the InnovationLab GmbH (Heidelberg) run by the authors. The spectrometer is equipped with a monochromatized Al Kα X-ray source and a concentric hemispherical analyzer. The approximate spot size for the XPS beam is 250−300 μm in diameter. The overall instrument resolution determined by the width of the Fermi edge of a freshly cleaned silver foil is 0.4 eV for XPS. Detailed spectra of the core-level lines were recorded with a pass energy of 11.75 eV. The spectra are referenced in binding energy with respect to the core-level lines of in situ cleaned Au, Ag, and Cu metal foils.

RESULTS AND DISCUSSION

Alq_3 Monolayer Growth Mechanism. Figure 1 shows the stepwise formation of Alq_3 monolayers in our MLD process. If it is not otherwise stated, then all growth processes occur at 80 °C (for further details, see the Experimental Section). Starting with a thin (typically 10 nm) Al_2O_3 layer prepared by ALD, in the first step the surface is functionalized with amino groups. To this end, the surface is sequentially exposed to (3-aminopropyl)triethoxysilane (APTES) and water until saturation in the growth is found,[18] as evidenced by in situ quartz crystal microbalance (QCM) measurements (Figure 2).

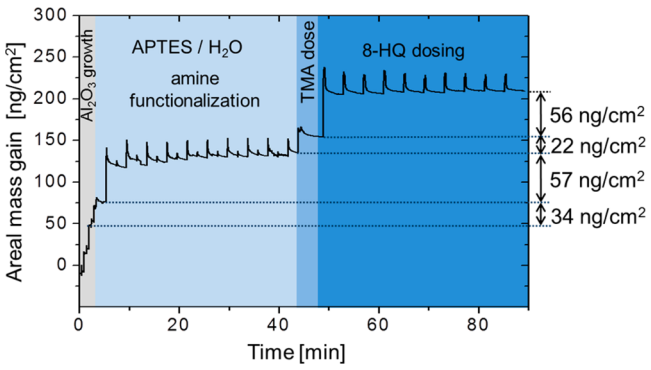

Figure 2. In situ quartz crystal microbalance monitoring of the mass gain during the respective growth steps of Alq_3 monolayer formation. The graph starts with the last few cycles of the Al_2O_3 deposition before amine functionalization.

Obviously, a saturated growth of the APTES on the surface was found, with the first APTES pulse accounting for most of the total areal mass gain of 57 ng/cm^2. This results in a rough estimate for the area density of amino groups of 4.1 1/nm^2, in reasonable agreement with previous reports of surfaces functionalized with APTES that showed a density of amino groups in the range of 2−61/nm^2.[19−21]

This amine functionalization is followed by the exposure to a single dose of TMA, and the corresponding mass gain was 22 ng/cm^2. The bond formation between TMA and amine groups was studied theoretically by Xu et al. using density functional calculations.[22] According to their work, the Al−N dative bond that forms as an initial step is stronger than the Al−O dative bond resulting from TMA adsorption at hydroxyl sites. From this dative Al−N bond, there is an energy barrier of 1.22 eV for the formation of a covalent Al−N bond, which is nearly twice as large as the barrier of the analogous reaction of TMA with −OH groups (0.65 eV). These theoretical calculations are in agreement with previous experimental results.[23] A similar dative bond has been predicted for TMA and triethylenediamine.[24] It has been estimated that to achieve the same reaction kinetics as in the TMA −OH case at 30 °C, the TMA $-NH_2$ system would require a processing temperature of >300 °C. On the basis of these considerations, it is very likely that at a reaction temperature of 80 °C the TMA molecules in our case bind datively to the $-NH_2$ groups without loss of their methyl groups (center of Figure 1). From the QCM data, we can estimate that after the single TMA pulse roughly half of all amino groups are occupied with TMA molecules. This result is strongly supported by the XPS analysis data presented later.

These datively bonded TMA molecules are then exposed to repeated doses of 8-HQ molecules. It is known that the reaction of TMA and 8-HQ leads to the formation of Alq_3 and methane as byproduct.[16] As can be seen in Figure 2, the dominating mass gain occurs during the first 8-HQ dose and rapidly tends to saturate upon subsequent exposures to 8-HQ. The entire mass gain is 56 ng/cm^2. From a very simple estimate, this means that in the saturated case there are roughly

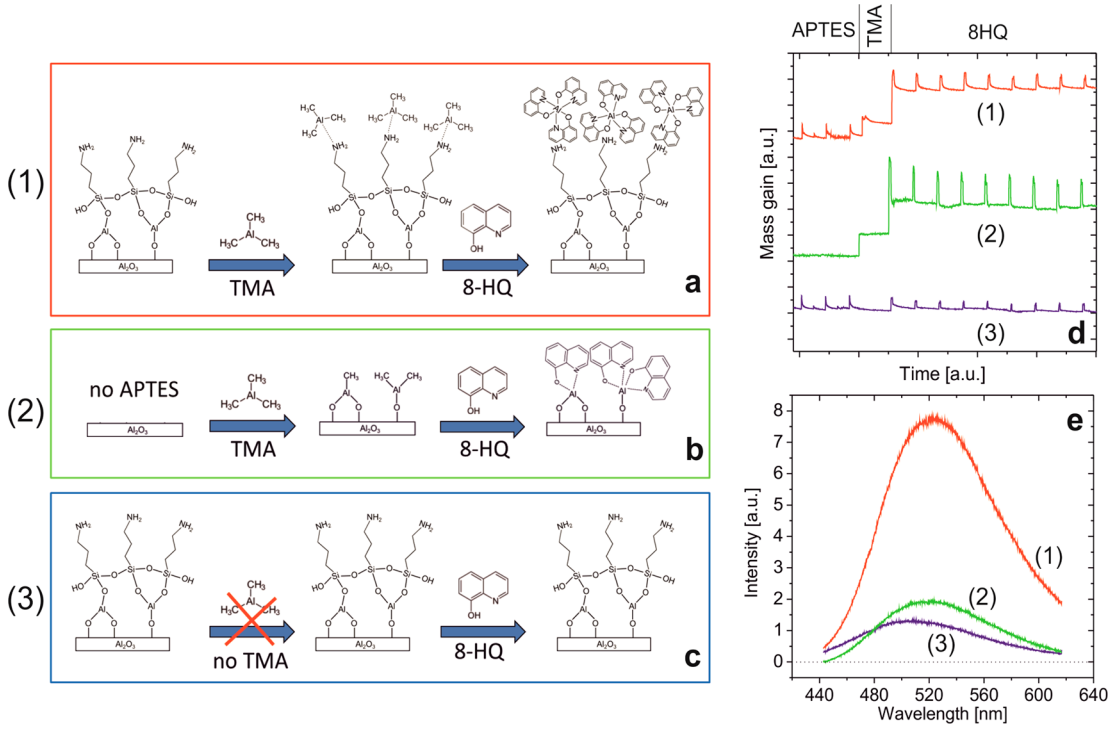

Figure 3. (a−c) Growth schemes of processes with deliberate variations (1−3). (d) Corresponding QCM mass gain (vertically offset for clarity). Note that the time axis starts with the last few APTES pulses. (e) PL data of the respective layers.

dx.doi.org/10.1021/am404918g | ACS Appl. Mater. Interfaces 2014, 6, 1193−1199

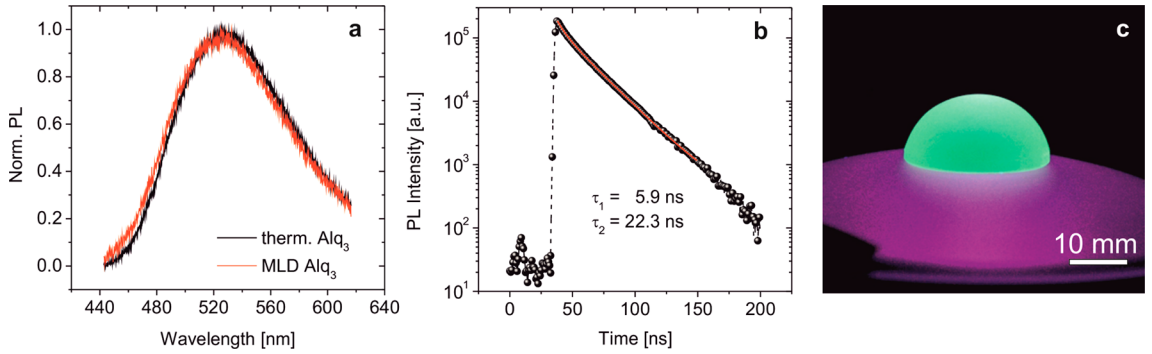

Figure 4. (a) Comparison of the normalized PL spectra of a thermally evaporated Alq_3 layer and the spectrum for an Alq_3 monolayer prepared by MLD (process 1 in Figure 3a). (b) Corresponding time-resolved PL of the Alq_3 monolayer. The red line is a biexponential fit to the measurement. (c) Photograph of the PL from a coated half-sphere excited with an UV–LED array (λ = 375 nm).

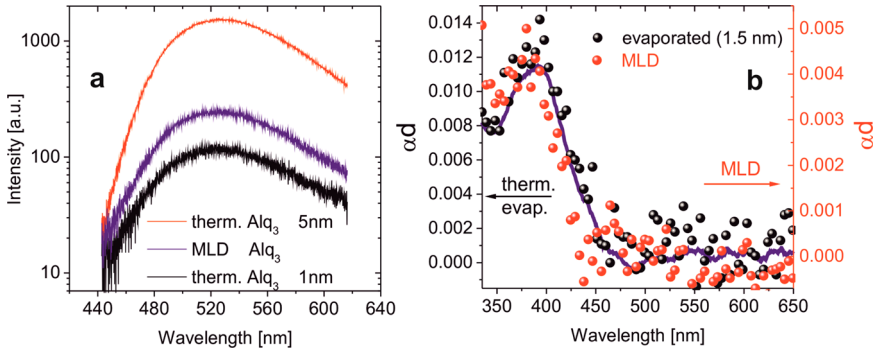

Figure 5. (a) PL spectra for the MLD Alq_3 samples compared to that of thermally deposited Alq_3 layers with a thickness of 1 and 5 nm, respectively. (b) Absorption spectra of the MLD Alq_3 layer compared to a thermally evaporated reference (thickness: 1.5 nm). The blue line is a guide to the eye.

two 8-HQ molecules per previously adsorbed TMA molecule. However, for Alq_3, three 8-HQ ligands per TMA molecule would be required. The difference may be discussed on the basis of sterical considerations. The diameter of a single Alq_3 molecule would be roughly 1 nm.[25] Therefore, in a monolayer of Alq_3 molecules, we would expect an area density of about 1–1.2 Alq_3 molecules/nm^2. This may explain the saturation of 8-HQ at a value that allows only $^2/_3$ of all TMA molecules to form Alq_3.

Morphological studies of the deposited layers using scanning electron microscopy (SEM) and atomic force microscopy (AFM) are shown in the Supporting Information (Figure S1). A variation of the substrate temperature in otherwise identical growth processes reveals that at the standard growth temperature of 80 °C smooth homogeneous layers are found (Figure S1a,c), whereas in the case of 150 °C substrate temperature, the pronounced formation of nanocrystallites is seen (Figure S1b,d). Layer homogeneity on length scales below the resolution of these techniques will have to be verified by other techniques with higher spatial resolution. Note that Alq_3 is well-known to form a rich variety of (nano)crystalline structures.[26,27] Optical emission microscopy confirms that the dominating contribution to the PL of the nanocrystal samples is directly associated with these crystals, whereas the sample surface is dark in between. Commonly, the crystal formation is accompanied by a spectral blue shift of the PL emission.[27] As shown in Figure S1f, we evidence a substantial blue shift of the PL maximum for all of the samples prepared at 150 °C (517 nm compared to 524 nm for the 80 °C samples) as a result of the formation of nanocrystallites. It is essential to note that in QCM the mass gain per area during the deposition at 80 and 150 °C is largely similar. This indicates that in the case of the 150 °C samples the equivalent of a monolayer of Alq_3 rearranges on the surface to form the observed nanocrystals. Our observations clearly show that the MLD-deposited Alq_3 molecules have a reasonable mobility on the APTES-functionalized surface, which allows for the observed self-assembly to the needle-like crystallites at the higher growth temperatures. We will focus our further studies in this article on noncrystallized Alq_3 layers prepared at 80 °C.

Optical Luminescence Spectroscopy. In an attempt to confirm experimentally the growth mechanism discussed in the previous section, we introduced the modifications schematically shown in Figure 3a–c. Process 1 is identical to what was already discussed, whereas in process 2, the amine functionalization with APTES was omitted. In a similar sense, in process 3, the TMA dose previous to the 8-HQ exposure is missing. The corresponding QCM mass gain is shown in Figure 3d, and the PL spectra are displayed in Figure 3e. Layers resulting from the complete process 1 show a strong green luminescence upon excitation with UV light (λ = 355 nm). The spectral maximum of 524 nm is in favorable agreement the PL spectrum of a thermally deposited Alq_3 thin film (Figure 4a) and agrees well with other previous reports for Alq_3 thin films.[28,29] In the case of a missing amine functionalization of the Al_2O_3 surface (2), 8-HQ can directly react with covalently bound $(CH_3)_xAl–O–$ surface species (x = 1 or 2). The resulting PL signal is significantly weaker compared to that found in the case of the complete process 1. The low PL intensity and the slightly blue-shifted PL spectrum (518 nm) is in line with reports on Alq_3 that has undergone hydrolysis to from Alq_2–OH species.[30] Finally, in the case of process 3, the 8-HQ is directly exposed to

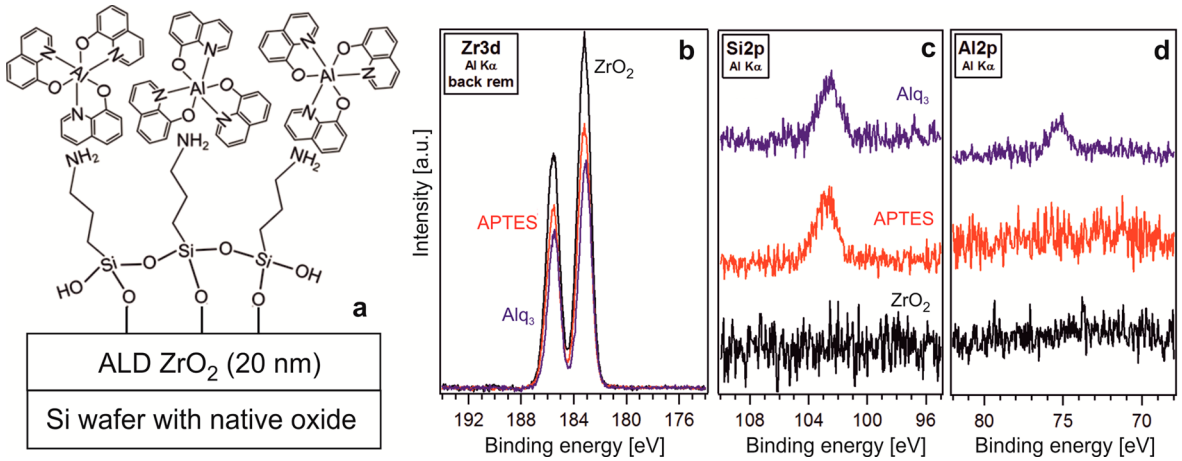

Figure 6. (a) Sample setup for the XPS analysis. (b) Zr 3d (with background subtracted), (c) Si 2p, and (d) Al 2p lines (vertically offset for clarity) acquired after the respective growth steps (ZrO_2, APTES, and Alq_3).

the amine-functionalized surface without a TMA dose in between. In this case, the mass gain because of the 8-HQ is below the resolution limit of the QCM. As a result, the PL of these samples is very weak, with a peak at 506 nm. The origin of this PL signal is not clear yet but may be due to some traces of 8-HQ that became deprotonated in a condensation reaction with residual Si−OH groups of the APTES-functionalization layer. Overall, the monolayer growth of Alq_3 of on top of amine-functionalized surfaces according to process 1 by far shows the brightest luminescence and spectral characteristics similar to Alq_3. To support further the validity of Alq_3 formation in process 1, we performed time-resolved PL measurements (Figure 4b). A biexponential fit yields two decay time constants (τ_1 = 5.9 ns and τ_2 = 22.3 ns), which agree well to PL lifetime data reported in previous work for thermally evaporated Alq_3 thin films.[31,32] Figure 4c demonstrates the PL of a coated half-sphere upon excitation with an UV−LED array (375 nm) and shows the applicability of the approach on even more complex and high-aspect-ratio (porous) surfaces, as shown later.

Alq_3 Layer Thickness. For an in-depth assessment of the thickness of the MLD grown Alq_3 films, optical and X-ray photoelectron spectroscopy (XPS) were used. The results from XPS were also used to study the growth mechanism in more detail.

Figure 5a shows PL measurements of the MLD layers in comparison to thermally evaporated Alq_3 films with varied layer thickness. Note that the substrates in these experiments are all identical (with the same APTES functionalization). From the PL intensity, a layer thickness of the MLD films close to 1 nm can be determined, whereas the 5 nm thick thermally evaporated layer already shows a substantially higher PL intensity.

The results of optical transmission/absorption spectroscopy are shown in Figure 5b. At a wavelength of 380 nm, the MLD Alq_3 layer leads to an optical absorption of 0.4% (referenced to glass/Al_2O_3/APTES and corrected for reflection, see the Experimental Section for details). Using Beer's law and the corresponding absorption coefficient of a reference Alq_3 layer (thickness 1.5 nm) prepared by thermal evaporation, a thickness of the MLD layer on the order of 0.5 nm was determined. Considering the uncertainty associated with the determination of the absorption because of these ultrathin layers, the agreement with the results from the PL measurements above is reasonable. Taken together, the results of the optical spectroscopy support the claim of the MLD films being monolayers of Alq_3 molecules.

The growth steps of the Alq_3 monolayer-deposition process were further studied by XPS. For this purpose, the layer sequence was slightly modified to allow for a quantitative analysis of the species deposited in each step. As shown in Figure 6a, the substrate (a silicon wafer with native oxide) was initially coated with 20 nm of ZrO_2 by ALD.

The absence of any Si 2p XPS signal (Figure 6c) verifies that the thickness of the ZrO_2 layer is enough to render the Si substrate invisible for the XPS measurement (i.e., thicker than 15−20 nm). In a second step, the ZrO_2 layer is functionalized with APTES, after which a Si 2p signal resulting from the Si atoms of the silane linker appears in XPS (Figure 6c). At the same time, the Zr 3d signal becomes damped because of the APTES layer on top (Figure 6b). After the subsequent completion of the process by the formation of Alq_3, an Al 2p signal was detected (Figure 6d) and some further weakening of the Zr 3d signal from the underlying ZrO_2 was evidenced (Figure 6b). Note that the corresponding N 1s signals (because of the amine group of the APTES and the heterocyclic 8-HQ) after the respective deposition steps can be found in the Supporting Information (Figure S2). From the damping of the Zr 3d signal after the APTES and the Alq_3 steps, thicknesses of 1.1 and 0.7 nm can be derived for the APTES and Alq_3 layers, respectively. Here, Beer's law was applied using the respective Zr 3d intensity ratios and calculated inelastic mean free paths (41 Å for APTES and 34 Å for Alq_3).[33] From the Si 2p and Al 2p spectra and by using previously reported cross sections,[34] we are able to derive a ratio of 0.45 for the number of Alq_3 molecules per APTES molecules. This is in excellent agreement with a ratio of TMA/APTES = 0.5 determined from the in situ QCM measurements presented earlier.

Coating High-Aspect-Ratio Nanoporous Substrates. A fundamental advantage of MLD processes in comparison to conventional thermal evaporation is the ability to uniformly coat high-aspect-ratio structures without issues of shadowing. Thereby, MLD paves the way to functionalize high-surface-area scaffolds like anodic alumina, cellulose paper, or aerogels for various applications. As a case study in this work, we used commercially available silica aerogels as template structures for an MLD process. Typical SiO_2 aerogels are characterized by a pore size on the order of 20 nm and BET surface area of about

200−800 m^2/g.[35] Their low material density and low effective refractive index results in their typical appearance as seen in Figure 7a. In comparison to this, the MLD-coated aerogel disk

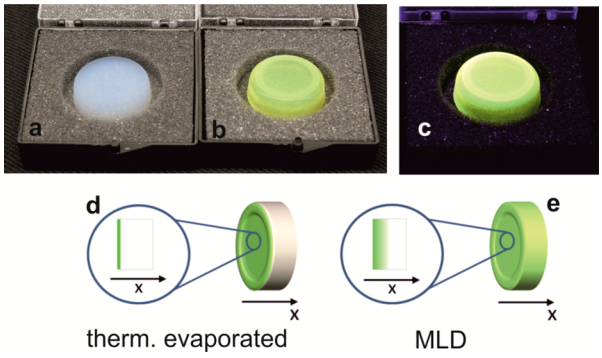

Figure 7. (a, b) Uncoated and coated pieces of silica aerogel under ambient light. (c) Luminescence of the coated aerogel upon illumination with UV light (λ = 375 nm). (d, e) Schematic difference of an aerogel coated with Alq_3 using thermal evaporation (d) or MLD (e). The zoomed-in area displays the coating depth of the aerogel in the vicinity of the surface for the two coating techniques. Whereas the thermal evaporation coats only the outer surface, for the MLD Alq_3, a coating depth of the porous aerogel volume between 8 and 30 μm was estimated (see the text for details).

appears yellowish because of the spectral-absorption characteristics of Alq_3 molecules (Figure 7b). Upon excitation with UV light, a strong green luminescence with the typical spectral characteristics of Alq_3 was found (Figure 7c).

The striking difference between conventional physical deposition techniques and MLD is schematically shown in Figure 7d,e. Thermally evaporated Alq_3 (thickness 200 nm) only coats the aerogel surface, resulting in a luminescent region confined to the sample surface (Figure 7d). In contrast, for the MLD-coated aerogel, the ability to coat porous structures without limitations of shadowing seeds the prospect that the MLD coating to some extent penetrates into the aerogel (Figure 7e). To quantify the extent of the penetration of the coating into the aerogel, we measured the effective transmission of an MLD-coated aerogel using a laser diode (λ = 405 nm, close to the maximum of the spectral absorption of Alq_3) and used an aerogel coated with 200 nm of Alq_3 by conventional thermal evaporation as a reference. As a result, we can estimate an effective thickness of the MLD layer of 600 nm, which corresponds roughly to about 600 monolayers. Taking the mass density of the aerogel of 0.095 g/cm^3 and the typical BET surface area of about 200−800 m^2/g,[35] we can estimate a penetration depth of the MLD-coating process into the aerogel of roughly 8−30 μm. Considering a typical pore size of 20 nm, this corresponds to an aspect ratio of 400−1500. The penetration depth will most likely be limited by clogging of the pores in deeper regions of the aerogel. Note that the thickness of the ALD-deposited layer before the APTES functionalization is 2 nm in this process.

As discussed in the Introduction, there are numerous applications of high-surface-area structures conformally coated with monolayers of luminescent molecules. Among them, the sensitizing of metal oxides opens avenues to dye-sensitized solar cells or photocatalysis. Because of its electronic structure, TiO_2 is the prototype metal oxide for these applications. Therefore, as a slight variation of the case shown in Figure 7 where the Alq_3 layers were grown on a thin Al_2O_3 layer underneath, we now used TiO_2 prepared by ALD instead of the Al_2O_3. Interestingly, whereas in the case with Al_2O_3 as underlayer a strong Alq_3 emission was found, this emission was almost entirely quenched in the case with a TiO_2 layer underneath (Figure 8a). This phenomenon can be understood

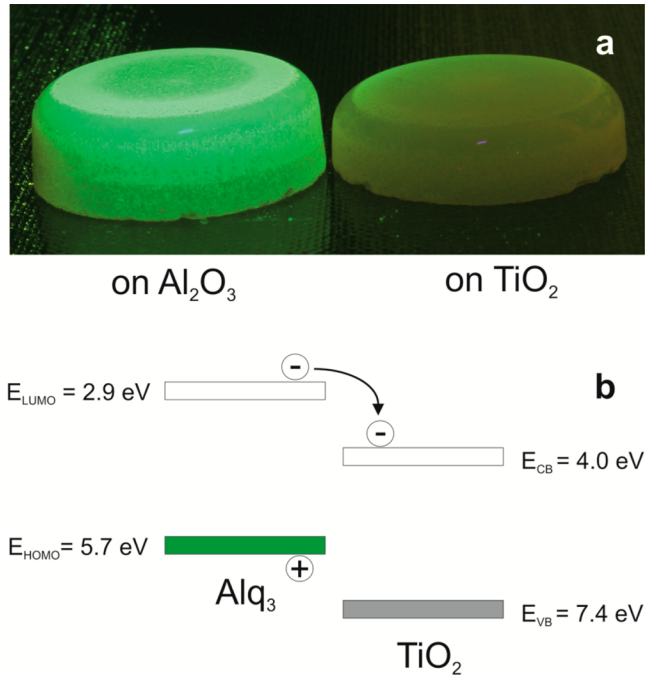

Figure 8. (a) Coated pieces of silica aerogel upon illumination with UV light (λ = 375 nm): (left) Al_2O_3/APTES/Alq_3 and (right) TiO_2/APTES/Alq_3. (b) Energy levels of Alq_3 and TiO_2 and schematic dissociation of photogenerated excitons on Alq_3 via electron transfer to TiO_2. For simplicity, the exciton binding energy of Alq_3 was neglected in this scheme.

when looking at the electronic structure of TiO_2 and Alq_3 (Figure 8b). The band data for TiO_2 and molecular levels for Alq_3 have been taken from the literature.[36,37] Possible interface dipoles and band bending are not considered in this simple sketch. Note that for a correct assessment of the excitonic energy levels of the organic compound the exciton binding energy for Alq_3 of typically 0.4 eV has to be taken into account.[38] As a result of the energy difference between the LUMO of Alq_3 and the conduction band of TiO_2 of about 1.1 eV, photogenerated excitons in the Alq_3 monolayer will be efficiently dissociated because of an energetically favored electron transfer to TiO_2.

Electrons transferred to the conduction band of TiO_2 are the prerequisite for photocatalytic surface reactions.[39] We note that the influence of the APTES layer on the level alignment between Al_2O_3 and TiO_2 was not taken into account in this discussion. In previous studies, the amine functional group was shown to lower the work function of metal oxides covered by self-assembled monolayers of APTES by roughly 0.5 eV.[40] These results seed the prospect of MLD being useful to form functionalized, high-surface-area structures via surface reactions from the gas phase.

CONCLUSIONS

The gas-phase molecular layer deposition of highly luminescent monolayers of Alq_3 was demonstrated. The utilization of dative

binding of trimethyl aluminum molecules on amino-functionalized surfaces allows, for the first time, a self-limiting surface reaction with 8-hydroxyquinoline to form a monolayer of Alq_3 molecules. The growth process and monolayer formation were studied and verified by in situ quartz crystal monitoring, optical emission and absorption spectroscopy, and X-ray photoelectron spectroscopy. The nature of the MLD process provides an avenue to coat arbitrarily shaped surfaces and porous structures with high surface areas, as demonstrated in this work for silica aerogels. The concept presented here will be applicable to other luminescent MLD systems and paves the way to highly sensitive luminescent sensors and dye-sensitized metal oxides for future applications in photocatalysis.

■ ASSOCIATED CONTENT

Supporting Information

AFM images of MLD samples prepared at 80 and 150 °C and corresponding scanning electron microscopy images, optical microscopy image of a 150 °C sample under UV excitation, normalized PL spectra of samples prepared at 80 °C and 150 °C, and additional XPS data. This material is available free of charge via the Internet at http://pubs.acs.org.

■ AUTHOR INFORMATION

Corresponding Author

*E-mail: t.riedl@uni-wuppertal.de.

Notes

The authors declare no competing financial interest.

■ ACKNOWLEDGMENTS

We are grateful to S. Adamczyk from the Department of Macromolecular Chemistry (University of Wuppertal, Germany) for carrying out the AFM measurements. We thank the German Federal Ministry for Education and Research (grant no. 13N11262) for financial support. P.G. acknowledges funding by the Emmy-Noether-Programm of the DFG (Deutsche Forschungsgemeinschaft).

■ REFERENCES

(1) O'Regan, B.; Graetzel, M. *Nature* **1991**, *353*, 737−740.
(2) Hagfeldt, A.; Graetzel, M. *Chem. Rev.* **1995**, *95*, 49−68.
(3) Basabe-Desmonts, L.; Reinhoudt, D. N.; Crego-Calama, M. *Chem. Soc. Rev.* **2007**, *36*, 993−1017.
(4) George, S. M. *Chem. Rev.* **2009**, *110*, 111−131.
(5) *Atomic Layer Deposition of Nanostructured Materials*; Pinna, N., Knez, M., Eds.; Wiley: Weinheim, Germany, 2012.
(6) Suntola, T. *Thin Solid Films* **1992**, *216*, 84−89.
(7) Levy, D. H.; Freeman, D.; Nelson, S. F.; Cowdery-Corvan, P. J.; Irving, L. M. *Appl. Phys. Lett.* **2008**, *92*, 192101-1−192101-3.
(8) Poodt, P.; Lankhorst, A.; Roozeboom, F.; Spee, K.; Maas, D.; Vermeer, A. *Adv. Mater.* **2010**, *22*, 3564−3567.
(9) George, S. M.; Yoon, B.; Dameron, A. A. *Acc. Chem. Res.* **2009**, *42*, 498−508.
(10) Yoshimura, T.; Tatsuura, S.; Sotoyama, W. *Appl. Phys. Lett.* **1991**, *59*, 482−484.
(11) Zhou, H.; Bent, S. F. *J. Vac. Sci. Technol., A* **2013**, *31*, 040801-1−040801-18.
(12) Lee, B. H.; Yoon, B.; Abdulagatov, A. I.; Hall, R. A.; George, S. M. *Adv. Funct. Mater.* **2013**, *23*, 532−546.
(13) Yoshimura, T.; Tatsuura, S.; Sotoyama, W.; Matsuura, A.; Hayano, T. *Appl. Phys. Lett.* **1992**, *60*, 268−270.
(14) Burtman, V.; Zelichenok, A.; Yitzchaik, S. *Angew. Chem., Int. Ed.* **1999**, *38*, 2041−2045.
(15) Nilsen, O.; Klepper, K.; Nielsen, H.; Fjellvaag, H. *ECS Trans.* **2008**, *16*, 3−14.
(16) Nilsen, O.; Haug, K. R.; Finstad, T.; Fjellvaag, H. *Chem. Vap. Deposition* **2013**, *19*, 174−179.
(17) Tang, C. W.; VanSlyke, S. A. *Appl. Phys. Lett.* **1987**, *51*, 913−915.
(18) Peng, Q.; Gong, B.; Parsons, G. N. *Nanotechnology* **2011**, *22*, 155601.
(19) Heiney, P. A.; Grüneberg, K.; Fang, J.; Dulcey, C.; Shashidhar, R. *Langmuir* **2000**, *16*, 2651−2657.
(20) Kurth, D. G.; Bein, T. *Langmuir* **1993**, *9*, 2965−2973.
(21) Krasnoslobodtsev, A.; Smirnov, S. *Langmuir* **2001**, *17*, 7593−7599.
(22) Xu, Y.; Musgrave, C. B. *Chem. Mater.* **2004**, *16*, 646−653.
(23) Sauls, F. C.; Interrante, L. V.; Jiang, Z. *Inorg. Chem.* **1990**, *29*, 2989−2996.
(24) George, S. M.; Yoon, B.; Hall, R. A.; Abdulagatov, A. I.; Gibbs, Z. M.; Lee, Y.; Seghete, D.; Lee, B. H. In *Atomic Layer Deposition of Nanostructured Materials*; Pinna, N., Knez, M., Eds.; Wiley: Weinheim, Germany, 2012; pp 83−107.
(25) Rajeswaran, M.; Blanton, T. N.; Tang, C. W.; Lenhart, W. C.; Switalski, S. C.; Giesen, D. J.; Antalek, B. J.; Pawlik, T. D.; Kondakov, D. Y.; Zumbulyadis, N.; Young, R. H. *Polyhedron* **2009**, *28*, 835−843.
(26) Cölle, M.; Gmeiner, J.; Milius, W.; Hillebrecht, H.; Brütting, W. *Adv. Funct. Mater.* **2003**, *13*, 108−112.
(27) Cho, C. P.; Wu, C. A.; Perng, T. P. *Adv. Funct. Mater.* **2006**, *16*, 819−823.
(28) Bi, H.; Zhang, H.; Zhang, Y.; Gao, H.; Su, Z.; Wang, Y. *Adv. Mater.* **2010**, *22*, 1631−1634.
(29) Baldacchini, G.; Baldacchini, T.; Chiacchiaretta, P.; Pace, A.; Pode, R. B. *J. Electrochem. Soc.* **2007**, *154*, J217−J225.
(30) Knox, J. E.; Halls, M. D.; Hratchian, H. P.; Bernhard Schlegel, H. *Phys. Chem. Chem. Phys.* **2006**, *8*, 1371−1377.
(31) Ravi Kishore, V. V. N.; Narasimhan, K. L.; Periasamy, N. *Phys. Chem. Chem. Phys.* **2003**, *5*, 1386−1391.
(32) Heiskanen, J. P.; Tolkki, A. E.; Lemmetyinen, H. J.; Hormi, O. E. O. *J. Mater. Chem.* **2011**, *21*, 14766−14775.
(33) Tanuma, S.; Powell, C. J.; Penn, D. R. *Surf. Interface Anal.* **1994**, *21*, 165−176.
(34) Yeh, J. J.; Lindau, I. *At. Data Nucl. Data Tables* **1985**, *32*, 1−155.
(35) Pierre, A.; Rigacci, A. In *Aerogels Handbook*; Aegerter, M. A., Leventis, N., Koebel, M. M., Eds.; Springer: New York, 2011; pp 21−45.
(36) Trost, S.; Zilberberg, K.; Behrendt, A.; Polywka, A.; Görrn, P.; Reckers, P.; Maibach, J.; Mayer, T.; Riedl, T. *Adv. Energy Mater.* **2013**, *3*, 1437−1444.
(37) Djurovich, P. I.; Mayo, E. I.; Forrest, S. R.; Thompson, M. E. *Org. Electron.* **2009**, *10*, 515−520.
(38) Krause, S.; Casu, M. B.; Scholl, A.; Umbach, E. *New J. Phys.* **2008**, *10*, 085001.
(39) Linsebigler, A. L.; Lu, G. Q.; Yates, J. T. *Chem. Rev.* **1995**, *95*, 735−758.
(40) Song, M.; Kang, J.-W.; Kim, D.-H.; Kwon, J.-D.; Park, S.-G.; Nam, S.; Jo, S.; Ryu, S. Y.; Kim, C. S. *Appl. Phys. Lett.* **2013**, *102*, 143303-1−143303-5.